J Appl Biotechnol Rep. 2019 June;6(2):60-68

Journal of
Applied Biotechnology Reports

doi 10.29252/JABR.06.02.04

Original Article

Developing a Novel Nanocomposite of Gold Nanowires/ Reduced Graphene Oxide/Molecularly Imprinted Polyaniline for the Electrochemical Sensing of Metronidazole

Mohammad Dehghani [1], Navid Nasirizadeh[2*], Mohammad Esmaeel Yazdanshenas[2]

[1]Young Researchers and Elite Club, Yazd Branch, Islamic Azad University, Yazd, Iran
[2]Department of Textile and Polymer Engineering, Yazd Branch, Islamic Azad University, Yazd, Iran

Corresponding Author: Navid Nasirizadeh, PhD, Associate Professor, Department of Textile and Polymer Engineering, Yazd Branch, Islamic Azad University, Yazd, Iran. Tel: +98-353-31872280, Fax: +98-351-8117550, Email: nasirizadeh@iauyazd.ac.ir

Received January 28, 2019; **Accepted** April 13, 2019; **Online Published** June 13, 2019

Abstract

Introduction: BIn the present study, a selective electrochemical sensor was developed to detect metronidazole (MTZ) through the modification of a screen-printed carbon electrode. Also, molecularly imprinted polyaniline (PANI) film layer/gold nanowire /reduced graphene oxide (GNW/rGO) was used to facilitate the charge transfer process and increase the specific surface area of the sensor.

Materials and Methods: The molecularly imprinted PANI electropolymerization process and MTZ accumulation on the electrode were optimized using the response surface method. The modified screen printed carbon electrode (SPCE) was characterized by scanning electron microscopy and electrochemical impedance spectroscopy (EIS).

Results: The performance of the proposed electrochemical sensor was analyzed, and it proved to have a linear range of 0.03–980.0 nmolL^{-1} and a detection limit of 0.015 nmolL^{-1}. The selectivity tests of the nanosensor showed its higher specificity for MTZ, as compared to other similar molecules. Furthermore, the developed sensor was successfully applied to detect MTZ in tablets and urine samples with a good recovery percentage.

Conclusions: In comparison with other methods of MTZ detection, the proposed MIP-based electrochemical sensor offers a wider linear response and a lower detection limit.

Keywords: Electrochemical Sensor, Metronidazole, Molecularly Imprinting, Gold Nanowire

Citation: Dehghani M, Nasirizadeh N, Yazdanshenas ME. Developing a novel nanocomposite of gold nanowires/reduced graphene oxide/ molecularly imprinted polyaniline for the electrochemical sensing of metronidazole. J Appl Biotechnol Rep. 2019;6(2):60-68. doi:10.29252/JABR.06.02.04.

Introduction

Metronidazole (MTZ: 1 beta-hydroxyethyl-2-methyl-5-nitromidazole), as a synthetic antibiotic belonging to the nitroimidazole class, is an antibacterial and anti-protozoal agent.[1] It is most widely used to treat infectious diseases caused by anaerobic bacteria and protozoa.[2] However, due to its ring structure, it can cause carcinogenic, teratogenic, mutagenic and genetic toxicities to humans.[3-5] Therefore, it is very important to develop highly sensitive and rapid methods for MTZ determination. For this purpose, a variety of analytical methods have been used so far, including different versions of high-performance liquid chromatography and ultra-performance liquid chromatography,[6-9] thin layer chromatography,[10,11] gas chromatography,[12,13] and spectrophotometry.[14,15]

The above-mentioned methods suffer from technical problems in drug separation and detection, such as being costly and time-consuming and needing large amounts of samples. Most importantly, separation of MTZ by those techniques needs purification and pre-concentration. In this context, electrochemical methods prove to be of benefit due to their low cost, simple operation, fast response, and ease of handling.[16-18]

Many researchers have reported that modification of electrodes by using nanoparticles and molecularly imprinted polymers (MIPs) is a key step to design, fabricate, and operate sensors and biosensors.[18-20] Nanomaterials can improve the sensitivity of nanosensors by enhancing the electron transfer rate and expanding the actual surface area of electrodes.[21-23] In addition, MIPs have advantages such as simplicity, low cost and high selectivity. At the same time, unlike other materials, they are effective even for ultra-trace quantities.[24,25] The MIP electrochemical sensors can be made in a variety of ways including bulk polymerization, sol-gel process,

electropolymerization, and layer-by-layer deposition.[26,27] Among these, electropolymerization is a simple, safe and more convenient way of fabricating MIP films directly on the surface of an electrode. The thickness and morphology of electropolymerized films can be controlled by adjusting the voltage and the number of cycles.[28] Polyaniline (PANI) as a conductive polymer is widely used in MIP-based electrochemical detection methods. It is also combined with nanomaterials to form a nanocomposite and pool the advantages of both MIP-PANI and nanomaterials.[29]

In this study, an electrochemical sensor was developed to determine MTZ by using molecularly imprinted PANI (MIP) combined with a gold nanowire (GNW)/reduced Graphene Oxide (rGO) modified screen printed carbon electrode (SPCE). The use of SPCEs offered such advantages as good reproducibility, low production cost, good thermal conductivity and electrical resistivity. Graphene oxide sheets are very good candidates for the fabrication of electrochemical sensors because they provide a 2D environment for electron transport with a high surface area, excellent conductivity and high mechanical strength.[30,31] Also, GNW with a large surface-to-volume ratio and excellent electrical conductivity are one of the most widely used metal particles for the construction of sensors.[32,33] The integration of SPCE with an MIP/GNW/rGO Nano composite led to the increase of the electrode area, improvement of its conductivity and sensitivity as well as an enhancement in the oxidation current response of MTZ. The fabrication procedure was assessed using field emission scanning electron microscopy (FESEM) and electrochemical impedance spectroscopy (EIS). In addition, the proposed sensor was applied to tablets and urine samples with satisfactory results.

Experimental

Materials

Reduced graphene oxide (rGO, 2.0 mgmL^{-1}) and gold nanowire (GNW, 2.0 mgmL^{-1}) dispersions were purchased from Sigma-Aldrich, USA. The other materials were purchased from MERCK, Germany.

Apparatus

Electrochemical measurements were performed by a PGSTAT101 (Autolab, the Netherlands) connected to a SPCE (Model DRP-C110) from Dropsens Co., Spain. In the SPCE system, the working, counter and reference electrodes were of carbon, platinum and silver respectively. Characterization through FESEM was done by a MIRA3 TESCAN instrument. The TEM images were taken for characterization using a Zeiss-EM10C-80 KV transmission electron microscope (Germany). Through the KBr method, the binding of MTZ molecules on the surface of the MIP-based sensor was demonstrated by means of a Fourier transform infrared spectrometer (FTIR) from Bruker Co., Germany.

Preparation of the MIP/GNW/GO/SPCE

The schematic diagram for the stepwise procedure of fabricating an MIP-based nanosensor is presented in Scheme 1. The surface of a SPCE working area was first cleaned using double distilled water, and then 2.5 µL of an rGO suspension was placed on it. The electrode was stored at room temperature until completely dried. Then, 3.0 µL of a GNW suspension was placed on the GO/SPCE, and the modified electrode was incubated in a humid container until completely dried (the obtained electrode was named 'GNW/rGO/SPCE'). Afterwards, the modified SPCE was placed in a solution containing 0.075 molL^{-1} HNO_3, 0.025 molL^{-1} H_2SO_4, 0.1 molL^{-1} aniline and 5.0 mmolL^{-1} MTZ. The aniline was electropolymerized by cyclic voltammetry at – 0.2 V to +1.0 V with the scan rate of 20 mVs^{-1} for five repeated cycles. After that, the prepared MIP-modified SPCE was washed with an ethanol/water mixture to dissolve and extract MTZ from the PANI matrix. After the extraction of MTZ, some pores remained in the PANI, known as molecular imprint (MIP). The resulting electrode was named 'MIP/GNW/rGO/SPCE'.

On the purpose of characterization, each of the above fabrication steps were followed by EIS in a 5.0 mmolL^{-1} $K_3[Fe(CN)_6]/K_4[Fe(CN)_6]$ containing 1.0 molL^{-1} KCl. Furthermore, FESEM imaging was performed for the nanoparticle-modified SPCE and the MIP-modified electrode.

Detection of MTZ

The MIP/GNW/rGO/SPCE was dipped in a 0.1 molL^{-1} phosphate buffer solution (pH 5.5) containing MTZ stirred at 100 rpm for 12 minutes. The electrochemical response of the MTZ molecules accumulated in the MIP deposited on the SPCE was measured by differential pulse voltammetry.

Results and Discussion

Fabrication of the developed nanosensor is explained in Scheme 1. As it is shown, a bare SPCE was modified with

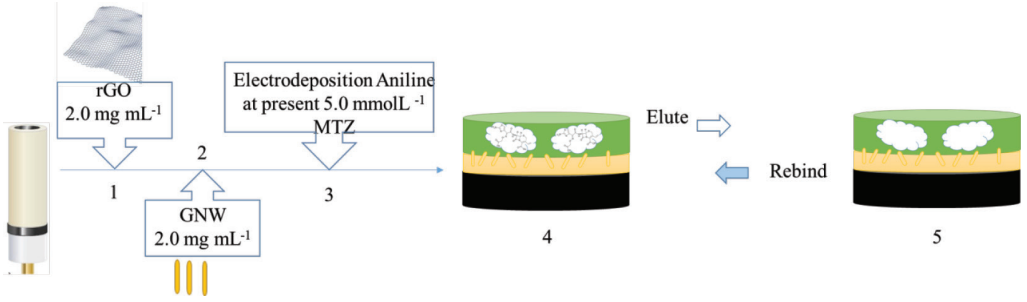

Scheme 1. Overview of the Steps of Fabricating the MTZ Nanosensor Based on Aniline MIP Layer Electropolymerization.

rGO and GNW. Then, aniline was electropolymerized using CVs on the surface of the GO/GNW modified SPCE. After the template MTZ molecules were washed, the formed MIPs were ready to collect MTZ molecules in every solution for pre-concentration as well as detection of MTZ using DPV. The FESEM imaging, as the main characterization method, was done in every modification step.

Modeling and Optimization of MTZ Determination

In MIP-based electrochemical sensing, it is necessary to optimize electropolymerization conditions and accumulation conditions. In this study, the number of cycles for electropolymerization, sample pH and accumulation time were optimized using the response surface methodology. The levels of the chosen variables are presented in Table 1.

Using this statistical method with the lowest number of experiments, an investigation was performed on the simultaneous effects of three significant variables on the response of the method suggested for the detection of MTZ through its oxidation signals. In addition, the results for the statistical optimization obtained through the designed experiments and ANOVA analysis are presented in Tables 2 and 3.

Table 1. Experimental Range and Levels of the Independent Variables

Parameters	Symbol	Levels				
		α-	-1	0	1	α
Cycles number	A	1	3	5	7	9
pH	B	2	4	7	10	12
Incubation time (min)	C	1	5	10	15	20

Table 2. Central Composite Design for the Maximum Oxidation Signal of MTZ by the Proposed Method

Run	A: Scan Cycle	B: pH	C: Accumulation Time	I
-	-	-	min	μA
1	5	7	10.5	9.14
2	5	7	10.5	7.8
3	5	7	10.5	6.8
4	3	4	15	2.51
5	5	7	10.5	8.95
6	5	2	10.5	3.53
7	9	7	10.5	8.23
8	1	7	10.5	2.54
9	3	10	5	1.56
10	7	10	15	5.55
11	5	7	10.5	10.25
12	5	7	1	0.09
13	3	4	5	2.7
14	7	4	5	6.7
15	3	10	15	2.94
16	7	10	5	0.02
17	5	12	10.5	2.45
18	7	4	15	6.74
19	5	7	20	9.07
20	5	7	10.5	10.7

Analysis of variance was done on the data to assay the interactions among them. The analysis was done using the design of experiment (DOE) software version 11.0.1 (Table 3). A *P* value less than 0.05 in the ANOVA table indicates the statistical significance of the proposed model at the confidence level of 95%. An F test was also applied to evaluate the statistical significance of all the terms in the polynomial equation at the confidence level of 95%. The results in the table point out to the encoded parameters A, B and C as the variables that affected the oxidation signal of MTZ on the proposed sensor. In addition, the interactions between variables A and B, A and C, and B and C had significant effects on the oxidation signal of MTZ. Based on the reported F values, variables C (accumulation time), A (scan cycle) and B (pH) had the most effects on the oxidation signal of MTZ.

The DOE software presents a second-order fitting equation for result modelling and result prediction. It also evaluates the model suitability using an ANOVA test. Therefore, the second-order polynomial equation should be expressed by equation (1):

$$I_{ox\ MTZ}\ (\mu A) = -17.76 + (3.29 \times scan\ cycle) + (3.66 \times pH) + (1.74 \times accumulation\ time) - (1.12 \times scan\ Cycle \times pH) + (1.04 \times scan\ cycle \times accumulation\ time) + (0.05 \times pH \times accumulation\ time) \quad \text{(Eq. 1)}$$

Variables A, B and C have positive effects on the oxidation signal of MTZ, but the effect of C is greater. This means that accumulation time has a better effect on the oxidation signal of MTZ. The above equation can be applied to predict the oxidation signal of MTZ with the proposed method within the range of the variables chosen.

Effects of Model Parameters and Their Interactions

An important advantage of the DOE software is its ability to produce three-dimensional (3D) response surface plots with which to illustrate the influence of individual variables and their interactions on the response.[29] The interactions between the three independent variables (i.e. the number of cycles for electropolymerization, sample pH and accumulation time) and the oxidation signal of MTZ as the dependent variable are presented in Figure 1.

Figure 1a shows the 3D plots of the simultaneous effects of the number of the CV cycles of the electropolymerization process and pH on the oxidation signal of MTZ within the accumulation time of 10 minutes. The highest current value was achieved with seven scan cycles. At lower potentials, the sensitivity declined, probably because of the formation of a non-uniform PANI and the decrease of the binding sites. The oxidation current was also reduced when excessive scan cycles were applied. This could be related to the low-conductive layer formed in the oxidization of PANI, which negatively affected the oxidation of MTZ.

In addition, the oxidation signal of MTZ steadily improved by the increase of pH from 3.0 to 6.5, but it reduced at pH 7.0 to 10.0. At lower pH values, the MTZ oxidation signal was the lowest, and it reached its peak at pH 6.5. Therefore, the interaction between MTZ and the PANI layer deposited on

Table 3. ANOVA Results and the Interactive Effects of the Variables on the Electrode Response to MTZ

Source	Sum of Squares	*df*	Mean Square	F Value	*P* value Prob > F	
Model	197.73	9	21.97	8.09	0.0015	Significant
A-scan cycle	26.07	1	26.07	9.61	0.0112	
B- pH	24.16	1	24.16	8.91	0.1184	
C-accumulation time	34.99	1	34.99	12.90	0.0049	
AB	6.4	1	6.4	9.36	0.1553	
AC	2.39	1	2.39	8.88	0.3693	
BC	6.23	1	6.23	9.29	0.1606	
A^2	26.32	1	26.32	9.70	0.0110	
B^2	69.63	1	69.63	25.66	0.0005	
C^2	38.57	1	38.57	14.21	0.0037	
Residual	27.12	10	2.71			
Lack of fit	16.39	5	3.27	1.52	0.327	Not significant
Pure error	10.73	5	2.14			
Cor total	224.86	19				

the SPCE could be due to the pK_a of MTZ, which was stated earlier as pK_a = 2.38 and PANI pK_a = 4.6.[34,35]

The functional group of PANI (i.e. NH_2) is protonated in acidic pH (pH < pK_a = 4.6), and MTZ has a partial positive charge in this condition. Therefore, the repulsive energy between a PANI film and MTZ inhibits appropriate interactions of MTZ molecules with PANI surface functional groups. As a result, in this study, MTZ molecules did not accumulate at the sensor surface to participate in redox reactions. The oxidation signal of MTZ was, thus, low. At a pH value close to 5.0, the hydroxyl group of MTZ (ROH) changed to (RO^-). Due to the attraction between the oppositely charged species, MTZ molecules were attracted to the active sites at the modified SPCE, and a proper interaction could occur between the hydroxyl group of MTZ and NH_2 at PANI, leading to the accumulation of MTZ on the surface of the sensor. Finally, these accumulated molecules participated in the redox reactions and produced a high analytical signal. On the other hand, in natural and basic environments, both the MTZ molecules and the active sites at the electrode surface (the functional group of PANI) had a partial negative charge; thus, the oxidation current of MTZ decreased due to the repulsion between them.

The simultaneous effect of the number of CV cycles of the electropolymerization process and the accumulation time on the oxidation signal of MTZ at pH 6.5 is shown in Figure 1b. As it can be seen, the MTZ oxidation signals improved by an increase in the time of MTZ accumulation on the modified SPCE, but the signals became stable after a while. It can be concluded that more MTZ molecules were accumulated in the binding sites formed at the modified nanosensor surface as the time went on. In other words, the MTZ molecules had enough time to interact with the PANI film.

The objective of the optimization was to determine optimum values for the variables and ultimately to achieve the highest oxidation signal of MTZ by the modified SPCE. As a result of optimization experiments, seven cycles of the CVs of electropolymerization, 12.0 minutes as the accumulation time and the pH of 5.5 were selected as the optimal conditions for the detection of MTZ. These conditions were then applied to

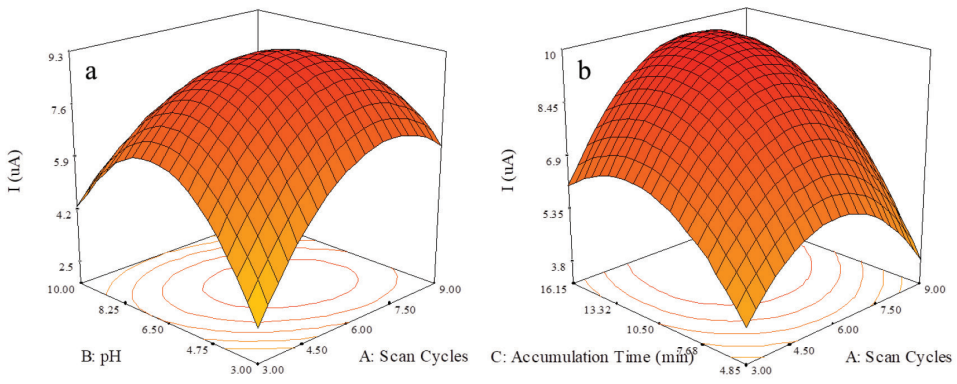

Figure 1. The 3D surface plots for the interaction effect of A) scan cycles and electrolyte pH (accumulation time was kept constant at 10 min) and B) scan cycles and accumulation time of electrode (pH was kept constant at 6.5) in a 100.0 nmol L^{-1} MTZ solution on the oxidation current of MTZ.

the experiments that were followed.

Characterization of the modified SPCE

The TEM images of rGO and GNW are presented in Figures 2a and 2b. According to Figure 2a, in terms of shape and layer form, the rGO sheets were found accurate enough for the modification of the SPCE. Furthermore, Figure 2b confirms the shape of the gold nanowires.

Figures 2c, 2d and 2e show the FESEM images of a GNW/ rGO/SPCE, an MIP/ GNW/rGO/ SPCE and an NIP/GNW/ rGO/SPCE. As it can be seen in Figure 2c, rGO makes a higher surface area, and GNW is dispersed on the graphene oxide sheet. Thus, the actual surface of the SPCE is vastly increased to amplify the signals and enhance the electron transfer. Indeed, rGO can serve as a widespread and suitable substrate for the immobilization of gold nanowires. This increases the interaction of GNW with rGO and causes fast and effective electron transfer between them.

The scanning electron microscopy (SEM) images of the SPCEs modified with MIP and NIP are presented in Figures 2d and 2e respectively. There is a substantial morphological difference between them. Compared to NIP (Figure 2e), the MIP surface (Figure 2d) contains more pores and has a rougher configuration. Actually, several deep cavities can be observed in the MIP surface. These cavities are formed by the dissolution and extraction of the MTZ molecules from the PANI matrix.

It can be mentioned that EIS is a suitable technique for understanding the interface characteristics of bare and modified electrode surfaces.[36] In order to evaluate the resistance of the electrode surface at different stages, the modified working electrode was immersed into a 0.1 $molL^{-1}$ phosphate buffer (pH 7.0) containing 1.0 $mmolL^{-1}$ $k_3[Fe(CN)_6]/k_4[Fe(CN)_6]$, and the corresponding Nyquist curve was plotted as shown in Figure 3. The diagonal diameter of the plots was equal to the charge transfer resistance (R_{ct}), and the electron transfer capacity decreased with the increment of the R_{ct} value.[37] As observed in plot *a*, the semicircle diameter of the Nyquist curve of the bare SPCE is very short. This suggests that there was not much restriction on the cleaned SPCE, and the electron transfer resistance was low. Also, the R_{ct} increased up to 2700 Ω after rGO immobilization (curve *b*). This could be well ascribed to the repellency of the redox probe from approaching the electrode surface by the repulsive force between GO with partially negative charges and $Fe(CN)_6]^{3-/4-}$ anions. Upon the deposition of gold nanowires on the surface of rGO/SPCE, due to the rapid kinetics of the electron transfer at the electrode surface modified with the GNW/rGO hybrid composite, R_{ct} dropped to 38 Ω (curve *c*). This behavior was predictable due to the high electrical conductivity of gold nanoparticles and the increase of the surface-to-volume ratio.

At the NIP or MIP/GNW/rGO/SCPE, after the electropolymerization of aniline, the R_{ct} slightly increased to 1340 Ω. This occurred due to the formation of a thin layer of poly-aniline on the GNW/rGO/SPCE surface and the prevented access of the electrolyte to the SPCE surface.

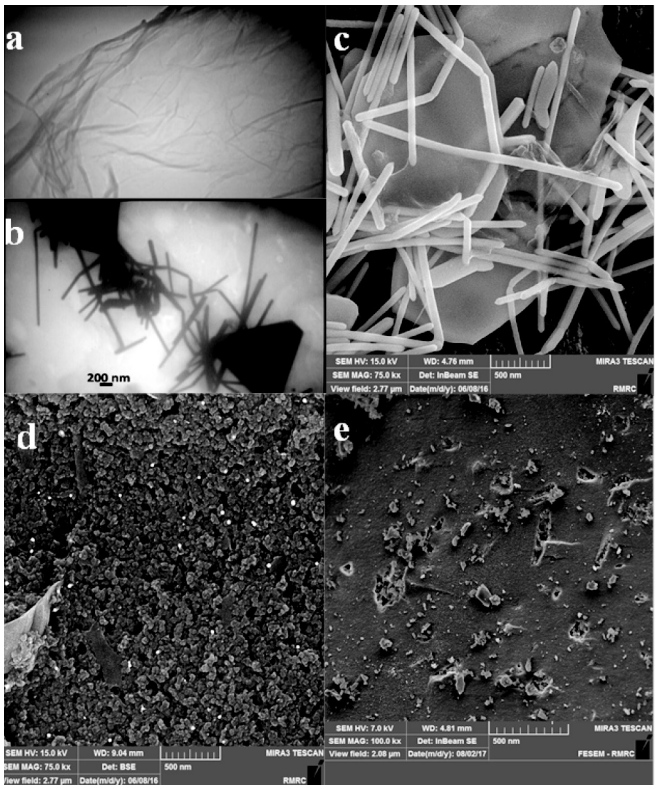

Figure 2. TEM images of (a) reduced graphene oxide and (b) gold nanowires. FESEM images of (c) SPCE surface modified with rGO/GNWs, (d) MIP/ GNW/ rGO/SPCE and (e) NIP/ GNW/rGO/SPCE.

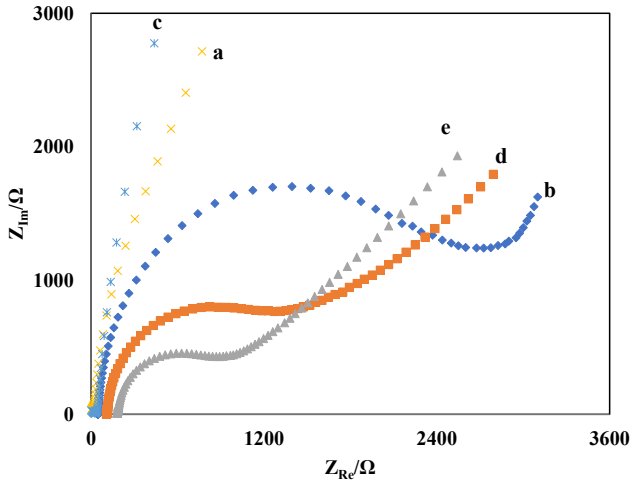

Figure 3. Nyquist Plots Of Different Sensors in a 1.0 $mmolL^{-1}$ $K_3Fe(CN)_6$ Solution: (a) bare SPCE, (b) rGO/ SPCE, (c) GNW/rGO/SPCE, (d) MIP/GNW/rGO/SPCE after polymerization, and (e) MIP/GNW/rGO/SPCE after template removal.

There was an apparent change in the electrochemical impedance spectrum after the removal of the template molecule (MIP) from the polymer matrix (curve *e* with the R_{ct} of 840 Ω). This change indicated a dramatic rise in the electron transfer rate caused by the creation of cavities in the film surface due to the extraction of MTZ molecules. It was through these cavities that the $Fe(CN)_6]^{3-/4-}$ anions, as electro-

active species, could have an access to the electrode surface.

In addition, the electrochemical performances of the MIP/GNW/rGO/SPCE were compared in the absence (curve a) and the presence (curve b) of 100.0 nmolL^{-1} MTZ by CV (Figure 4). As it can be seen, there is a considerable difference between the two curves in terms of peak signal intensity. In the absence of MTZ, no peak exists, which makes one conclude that all the MTZ molecules are removed from the MIP matrix through washing with an ethanol/water mixture. On the other hand, in the presence of MTZ, there is a peak at 0.59 V, which can be a sign of MTZ accumulation in the MIP imprints and the redox activity of the MTZ molecules.

Determination of MTZ

The performance of the MIP/GNW/rGO/SPCE to detect MTZ was assayed using DPV in different MTZ concentrations, as shown in Figure 5. In addition, the calibration plots of MTZ concentrations versus the oxidation signal of MTZ were drawn, as depicted in the inset of Figure 5. The oxidation signal of MTZ was measured after its accumulation on the MIP/GNW/rGO/SPCE. As it can be seen, in the MTZ concentration range of 0.03 nmolL^{-1}-980.0 nmolL^{-1}, the relationship of the oxidation signal to the MTZ concentration was linear. Therefore, the range of those MTZ concentrations was defined as a linear range. In addition, based on a previously reported method,[29] the limit of detection was found to be 0.015 nmolL^{-1}.

The analytical performance of the proposed method was compared to that of other methods previously reported for the determination of MTZ. As it can be concluded from Table 4, the proposed electrochemical sensor is superior in almost every aspect to most of those ever fabricated.[38-43] This might be attributed to the application of the MIP/GNW/rGO hybrid nanocomposite on the SPCE electrode.

Selectivity and Reproducibility

The specificity of the proposed sensor was assessed using materials with similar chemical structures and other species with a redox activity, such as nilutamide, 4-nitrobenzene, flutamide, 4-nitroaniline, 4-nitrophenol, glucose, uric acid, dopamine, ascorbic acid, and glutaric acid. Figure 6 shows the comparison of the responses of the prepared nanosensor in the presence of MTZ and the other mentioned molecules. As it can be seen, there is a big difference between the oxidation signal of MTZ and those of the other molecules. This proves that MIP/GNW/rGO/SPCEs have a high selectivity for recognizing MTZ. It can be also concluded that the cavities created in the PANI matrix act in a specific manner, and only MTZ molecules are capable of being inserted into the template.

To assess the reproducibility of the nanosensor, four MIP/GNW/rGO/SPCEs were prepared separately with

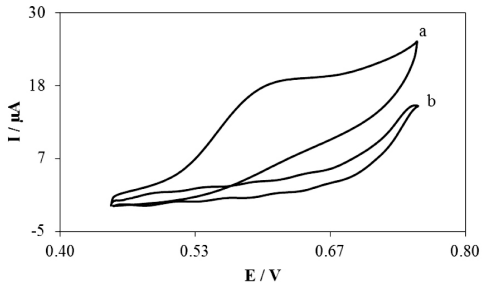

Figure 4. Cyclic Voltammograms of MIP/GNW/rGO/SPCE in (a) the Absence and (b) the Presence of 100.0 nmolL^{-1} MTZ.

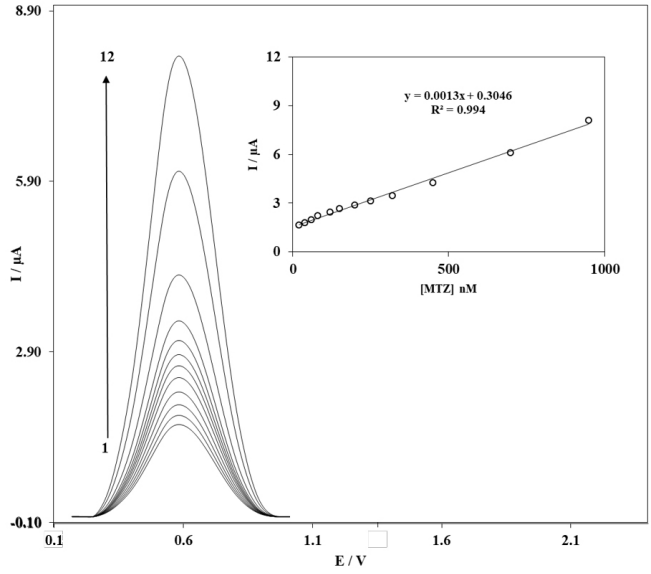

Figure 5. Differential Pulse Voltammograms of the MIP/GNW/rGO/ SPCE After Incubation in Different Concentrations of MTZ. Inset: calibration curve of the MIP/GNW/rGO/ SPCE in the concentration range of 0.03-980.0 nM

Table 4. Comparison of Some Analytical Parameters Involved in the Quantitative Determination of MTZ Using the Proposed Nanosensor and Some Other Sensors

Electrode	Technique	Linear Range (molL^{-1})	LOD (molL^{-1})	Real Sample	Reference
MIP/GNW/rGO/SPCE	DPV	0.03×10^{-9}-980.0 10×$^{-9}$	0.015×10^{-9}	Tablet and urine	This study
Pt nanospheres/polyfurfural film/GCE	DPV	2.5 10^{-6}-500× 10×$^{-6}$	50 10×$^{-9}$	Human serum	[38]
SrV_2O_6 /GCE	DPV	0.01 10^{-6}-207× 10×$^{-6}$	4 10×$^{-9}$	-	[39]
polydopamine/COOH-MWCNT/GCE	DPV	5 10^{-6}-5000× 10×$^{-6}$	0.25 10×$^{-6}$	Tablet	[40]
Cysteine/GE	DPV	50 10^{-6}-300× 10×$^{-6}$	2.6 10×$^{-6}$	Tablet	[41]
3D-HPG/PTH/(GCE)	DPV	0.05 10^{-9}×10^{-9}-70× 70×10^{-9}-500×10^{-9}	1.0 10×$^{-9}$	Water-tablets	[42]
Activated SPCE	DPV	0.05 10^{-6}× - 563 10^{-6}× 753 10^{-6}× - 2873 10×$^{-6}$	0.01 10×$^{-6}$	-	[43]

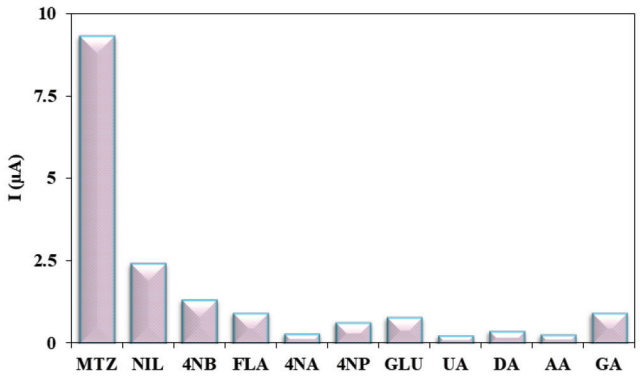

Figure 6. Signal Change Versus 600.0 nmolL-1 MTZ in the Presence of Co-existing Species.

85.0 nmolL^{-1} MTZ accumulated on them. The DPVs of the electrodes were recorded as in the previous sections. The mean and the relative standard deviation (RSD) were found to be 71 nA ± 1.7 and 2.3% respectively. A low RSD value can, indeed, be a good proof for the reproducibility of a nanosensor preparation method.

Testing the Real Samples

To confirm the reliability of the proposed method, MTZ was analyzed in tablets and urine samples. The urine samples were diluted 10 times with a 0.1 molL^{-1} phosphate buffer at pH 5.5 and then used as real samples. Certain spike concentrations were also added to the samples in microliter volumes. The measurements were performed in three replications, and their RSD were calculated for each concentration.

Table 5 shows the results of the tests. It presents information about the initial measurement, amount of spiking and rate of detection after spiking. As it can be seen, the recovery percentages are fairly near 100%, and their relative standard deviations are low. These results suggest that the nanosensor can be applied in future clinical studies for separation and or detection of MTZ in real samples.

Conclusions

In this study, a novel electrochemical nanosensor was developed based on a SPCE modified with an MIP/GNW/rGO nanocomposite to separate and quantify MTZ. The nanocomposite was prepared by electropolymerization to enhance the signals of the nanosensor as well as its capability of MTZ detection. In analytical experiments, the nanosensor proved to have a wide linear range from 0.03 nmolL^{-1} to 980.0 nmol L^{-1} and a LOD of 0.015 nmolL^{-1} for MTZ measurement. The sensor was used to separate and quantify MTZ in tablets and urine samples. It also had good performance in simulated samples. In comparison with other methods of MTZ detection, the proposed MIP-based electrochemical sensor offers a wider linear response and a lower detection limit. It also involves no expensive amplification or separation techniques. The sensor claims to be of practical applications as it has been successfully applied to detect MTZ in tablets and urine samples.

Table 5. The Recovery Percentages Obtained for the Quantitative Determination of Spiked MTZ in Tablets and Urine Samples (n = 3) Using an MIP/GNW/rGO/SPCE

Sample	Founded in sample (nmolL^{-1})	Added (nmolL^{-1})	Founded (nmolL^{-1})	Recovery (%)
Tablet	410.0	100.0	516.6	101.3
		200.0	605.4	99.2
		300.0	728.5	102.6
Urine	0.52	1.0	1.49	98.1
		2.5	3.06	101.6
		5.0	5.39	97.8

Authors' Contributions

All authors equally contributed to the current study.

Conflict of Interest Disclosures

The authors declare they have no conflicts of interest.

References

1. Yazdanbakhsh AR, Manshouri M, Sheikhmohammadi A, Sardar M. Investigation the Efficiency of Combined Coagulation and Advanced Oxidation by Fenton Process in the Removal of Clarithromycin Antibiotic COD. Water and Wastewater. 2012;23(2):22-29. [Persian].
2. Zhang H, Liu P, Feng Y, Yang F. Fate of antibiotics during wastewater treatment and antibiotic distribution in the effluent-receiving waters of the Yellow Sea, northern China. Mar Pollut Bull. 2013;73(1):282-290. doi:10.1016/j.marpolbul.2013.05.007.
3. Cheng H, Hong PY. Removal of antibiotic-resistant bacteria and antibiotic resistance genes affected by varying degrees of fouling on anaerobic microfiltration membranes. Environ Sci Technol. 2017;51(21):12200-12209. doi:10.1021/acs.est.7b03798.
4. Nasuhoglu D, Rodayan A, Berk D, Yargeau V. Removal of the antibiotic levofloxacin (LEVO) in water by ozonation and TiO2 photocatalysis. Chem Eng J. 2012;189-190:41-48. doi:10.1016/j.cej.2012.02.016.
5. Manjunath SV, Kumar SM, Ngo HH, Guo W. Metronidazole removal in powder-activated carbon and concrete-containing graphene adsorption systems: Estimation of kinetic, equilibrium and thermodynamic parameters and optimization of adsorption by a central composite design. J Environ Sci Health A Tox Hazard Subst Environ Eng. 2017;52(14):1269-1283. doi:10.1080/10934529.2017.1357406.
6. Jafarzadeh N, Rezazadeh H, Ramezani Z, et al. Taguchi optimization approach for metronidazole removal from aqueous solutions by using graphene oxide functionalized beta-cyclodextrin/Ag nanocomposite. Water Sci Technol. 2017;2017(1):36-47. doi:10.2166/wst.2018.080.
7. Shemer H, Kunukcu YK, Linden KG. Degradation of the pharmaceutical metronidazole via UV, Fenton and photo-Fenton processes. Chemosphere. 2006;63(2):269-276. doi:10.1016/j.chemosphere.2005.07.029.
8. Wang H, Zhang G, Gao Y. Photocatalytic degradation of metronidazole in aqueous solution by niobate $K_6Nb_{10.8}O_{30}$. Wuhan Univ J Nat Sci. 2010;15(4):345-349. doi:10.1007/s11859-010-0664-0.
9. Hammad Khan M, Jung JY. Ozonation catalyzed by homogeneous and heterogeneous catalysts for degradation of DEHP in aqueous phase. Chemosphere. 2008;72(4):690-696. doi:10.1016/j.chemosphere.2008.02.037.
10. Harrelkas F, Paulo A, Alves MM, et al. Photocatalytic and combined anaerobic-photocatalytic treatment of textile

dyes. Chemosphere. 2008;72(11):1816-1822. doi:10.1016/j.chemosphere.2008.05.026.
11. Alvarez JA, Otero L, Lema JM, Omil F. The effect and fate of antibiotics during the anaerobic digestion of pig manure. Bioresour Technol. 2010;101(22):8581-8586. doi:10.1016/j.biortech.2010.06.075.
12. Klavarioti M, Mantzavinos D, Kassinos D. Removal of residual pharmaceuticals from aqueous systems by advanced oxidation processes. Environ Int. 2009;35(2):402-417. doi:10.1016/j.envint.2008.07.009.
13. Taokaenchan N, Tangkuaram T, Pookmanee P, Phaisansuthichol S, Kuimalee S, Satienperakul S. Enhanced electrogenerated chemiluminescence of tris(2,2′-bipyridyl)ruthenium(II) system by l-cysteine-capped CdTe quantum dots and its application for the determination of nitrofuran antibiotics. Biosens Bioelectron. 2015;66:231-237. doi:10.1016/j.bios.2014.11.030.
14. Kathriarachchi UL, Vidhate SS, Al-Tannak N, Thomson AH, da Silva Neto MJJ, Watson DG. Development of a LC-MS method for simultaneous determination of amoxicillin and metronidazole in human serum using hydrophilic interaction chromatography (HILIC). J Chromatogr B Analyt Technol Biomed Life Sci. 2018;1089:78-83. doi:10.1016/j.jchromb.2018.05.012.
15. Astasov-Frauenhoffer M, Braissant O, Hauser-Gerspach I, et al. Microcalorimetric determination of the effects of amoxicillin, metronidazole, and their combination on in vitro biofilm. J Periodontol. 2014;85(2):349-357. doi:10.1902/jop.2013.120733.
16. Nasirizadeh N, Shekari Z, Dehghani M, Makarem S. Delphinidin immobilized on silver nanoparticles for the simultaneous determination of ascorbic acid, noradrenalin, uric acid, and tryptophan. J Food Drug Anal. 2016;24(2):406-416. doi:10.1016/j.jfda.2015.11.011.
17. Huang J, Shen X, Wang R, Zeng Q, Wang L. A highly sensitive metronidazole sensor based on a Pt nanospheres/polyfurfural film modified electrode. RSC Adv. 2017;7(1):535-542. doi:10.1039/C6RA25106D.
18. Ammar HB, Brahim MB, Abdelhedi R, Samet Y. Boron doped diamond sensor for sensitive determination of metronidazole: Mechanistic and analytical study by cyclic voltammetry and square wave voltammetry. Mater Sci Eng C Mater Biol Appl. 2016;59:604-610. doi:10.1016/j.msec.2015.10.025.
19. Yuan L, Jiang L, Hui T, et al. Fabrication of highly sensitive and selective electrochemical sensor by using optimized molecularly imprinted polymers on multi-walled carbon nanotubes for metronidazole measurement. Sens Actuators B Chem. 2015;206:647-652. doi:10.1016/j.snb.2014.10.019.
20. Liu P, Zhang X, Xu W, Guo C, Wang S. Electrochemical sensor for the determination of brucine in human serum based on molecularly imprinted poly-o-phenylenediamine/SWNTs composite film. Sens Actuators B Chem. 2012;163(1):84-89. doi:10.1016/j.snb.2012.01.011.
21. Kong L, Jiang X, Zeng Y, Zhou T, Shi G. Molecularly imprinted sensor based on electropolmerized poly(o-phenylenediamine) membranes at reduced graphene oxide modified electrode for imidacloprid determination. Sens Actuators B Chem. 2013;185:424-431. doi:10.1016/j.snb.2013.05.033.
22. Jafari S, Dehghani M, Nasirizadeh N, Akrami HR. Voltammetric determination of Basic Red 13 during its sonoelectrocatalytic degradation. Mikrochim Acta. 2017;184(11):4459-4468. doi:10.1007/s00604-017-2482-y.
23. Jafari S, Nasirizadeh N, Dehghani M. Developing a highly sensitive electrochemical sensor using thiourea-imprinted polymers based on an MWCNT modified carbon ceramic electrode. J Electroanal Chem. 2017;802:139-146. doi:10.1016/j.jelechem.2017.08.043.
24. Rao H, Chen M, Ge H, et al. A novel electrochemical sensor based on Au@PANI composites film modified glassy carbon electrode binding molecular imprinting technique for the determination of melamine. Biosens Bioelectron. 2017;87:1029-1035. doi:10.1016/j.bios.2016.09.074.
25. Shojaei S, Nasirizadeh N, Entezam M, Koosha M, Azimzadeh M. An electrochemical nanosensor based on molecularly imprinted polymer (MIP) for detection of gallic acid in fruit juices. Food Anal Methods. 2016;9(10):2721-2731. doi:10.1007/s12161-016-0459-9.
26. Zhang W, Zong L, Geng G, Li Y, Zhang Y. Enhancing determination of quercetin in honey samples through electrochemical sensors based on highly porous polypyrrole coupled with nanohybrid modified GCE. Sens Actuators B Chem. 2018;257:1099-1109. doi:10.1016/j.snb.2017.11.059.
27. Deiminiat B, Rounaghi GH. Fabrication of a new electrochemical imprinted sensor for determination of ketamine based on modified polytyramine/sol-gel/f-MWCNTs@AuNPs nanocomposite/pencil graphite electrode. Sens Actuators B Chem. 2018;259:133-141. doi:10.1016/j.snb.2017.12.062.
28. Menon S, Jesny S, Girish Kumar K. A voltammetric sensor for acetaminophen based on electropolymerized-molecularly imprinted poly(o-aminophenol) modified gold electrode. Talanta. 2018;179:668-675. doi:10.1016/j.talanta.2017.11.074.
29. Jafari S, Dehghani M, Nasirizadeh N, Azimzadeh M. An azithromycin electrochemical sensor based on an aniline MIP film electropolymerized on a gold nano urchins/graphene oxide modified glassy carbon electrode. J Electroanal Chem. 2018;829:27-34. doi:10.1016/j.jelechem.2018.09.053.
30. Dehghani M, Nasirizadeh N, Yazdanshenas ME. Determination of cefixime using a novel electrochemical sensor produced with gold nanowires/graphene oxide/electropolymerized molecular imprinted polymer. Mater Sci Eng C Mater Biol Appl. 2019;96:654-660. doi:10.1016/j.msec.2018.12.002.
31. Azimzadeh M, Rahaie M, Nasirizadeh N, Ashtari K, Naderi-Manesh H. An electrochemical nanobiosensor for plasma miRNA-155, based on graphene oxide and gold nanorod, for early detection of breast cancer. Biosens Bioelectron. 2016;77:99-106. doi:10.1016/j.bios.2015.09.020.
32. Wu Y. Electrocatalysis and sensitive determination of Sudan I at the single-walled carbon nanotubes and iron(III)-porphyrin modified glassy carbon electrodes. Food Chem. 2010;121(2):580-584. doi:10.1016/j.foodchem.2009.12.051.
33. Gholivand MB, Torkashvand M. A novel high selective and sensitive metronidazole voltammetric sensor based on a molecularly imprinted polymer-carbon paste electrode. Talanta. 2011;84(3):905-912. doi:10.1016/j.talanta.2011.02.022.
34. Tolls J. Sorption of veterinary pharmaceuticals in soils: a review. Environ Sci Technol. 2001;35(17):3397-3406. doi:10.1021/es0003021.
35. Jang J, Ha J, Lim B. Synthesis and characterization of monodisperse silica–polyaniline core–shell nanoparticles. Chem Commun. 2006(15):1622-1624. doi:10.1039/B600167J.
36. Hajihosseini S, Nasirizadeh N, Hejazi MS, Yaghmaei P. A sensitive DNA biosensor fabricated from gold nanoparticles and graphene oxide on a glassy carbon electrode. Mater Sci Eng C Mater Biol Appl. 2016;61:506-515. doi:10.1016/j.msec.2015.12.091.
37. Aghili Z, Nasirizadeh N, Divsalar A, Shoeibi S, Yaghmaei P. A nanobiosensor composed of Exfoliated Graphene Oxide and Gold Nano-Urchins, for detection of GMO products. Biosens Bioelectron. 2017;95:72-80. doi:10.1016/j.bios.2017.02.054.
38. Huang J, Shen X, Wang R, Zeng Q, Wang L. A highly sensitive metronidazole sensor based on a Pt nanospheres/polyfurfural film modified electrode. RSC Adv. 2017;7(1):535-542. doi:10.1039/C6RA25106D.
39. Karthik R, Kumar JV, Chen SM, Kumar PS, Selvam V, Muthuraj V. A selective electrochemical sensor for caffeic acid and photocatalyst for metronidazole drug pollutant - A dual role by rod-like SrV2O6. Sci Rep. 2017;7(1):7254. doi:10.1038/s41598-017-07423-1.

40. Tursynbolat S, Bakytkarim Y, Huang J, Wang L. Ultrasensitive electrochemical determination of metronidazole based on polydopamine/carboxylic multi-walled carbon nanotubes nanocomposites modified GCE. J Pharm Anal. 2018;8(2):124-130. doi:10.1016/j.jpha.2017.11.001.
41. Huayhuas-Chipana BC, Gomero JCM, Sotomayor MDPT. Nanostructured screen-printed electrodes modified with self-assembled monolayers for determination of metronidazole in different matrices. J Braz Chem Soc. 2014;25(9):1737-1745. doi:10.5935/0103-5053.20140170.
42. Mei Y, Guo M, Feng Y, et al. Sensitive Voltammetric Detection of Metronidazole Based on Three-Dimensional Graphene-Like Carbon Architecture/Polythionine Modified Glassy Carbon Electrode. J Electrochem Soc. 2018;165(11):B530-B535. doi:10.1149/2.1311811jes.
43. Sundaresan P, Chen TW, Chen SM, Tseng TW, Liu X. Electrochemical activation of screen printed carbon electrode for the determination of antibiotic drug metronidazole. Int J Electrochem Sci. 2018;13(2):1441-1451. doi:10.20964/2018.02.05.